Formation of a Complex of the Catalytic Subunit of Pyruvate Dehydrogenase Phosphatase Isoform 1 (PDP1c) and the L2 Domain Forms a Ca^{2+} Binding Site and Captures PDP1c as a Monomer†

Ali Turkan,‡ Yasuaki Hiromasa, and Thomas E. Roche*

Department of Biochemistry, Kansas State University, Manhattan, Kansas 66506

Received May 28, 2004; Revised Manuscript Received August 28, 2004

ABSTRACT: Pyruvate dehydrogenase phosphatase isoform 1 (PDP1) is a heterodimer with a catalytic subunit (PDP1c) and a regulatory subunit (PDP1r). The activities of PDP1 or just PDP1c are greatly increased by Ca^{2+}-dependent binding to the L2 (inner lipoyl) domain of the dihydrolipoyl acetyltransferase (E2) core. Using EGTA-Ca buffers, the dependence of PDP1 or PDP1c on the level of free Ca^{2+} was evaluated in activity and L2 binding studies. An increase in the Mg^{2+} concentration decreased the Ca^{2+} concentration required for half-maximal activation of PDP1 from 3 to 1 μM, but this parameter was unchanged at 3 μM with PDP1c. Near 1 μM Ca^{2+}, tight binding of PDP1 but not PDP1c to gel-anchored L2 required Mg^{2+}. With just Ca^{2+} included, some PDP1c separated from PDP1r and remained more tightly bound to L2 than intact PDP1. Thus, formation of the PDP1c·Ca^{2+}·L2 complex is supported by micromolar Ca^{2+} concentrations and becomes sensitive to the Mg^{2+} level when PDP1c is bound to PDP1r. Sedimentation velocity and equilibrium studies revealed that PDP1c exists as a reversible monomer/dimer mixture with an equilibrium dissociation constant of 8.0 ± 2.5 μM. L2 binds tightly and preferentially to the PDP1c monomer. Approximately 45 PDP1c monomers bind to the E2 60mer with a K_d of ~0.3 μM. Isothermal titration calorimetry and $^{45}Ca^{2+}$ binding studies failed to detect binding of Ca^{2+} (<100 μM) to L2 or PDP1c, alone, but readily detected binding to L2 and PDP1c. Therefore, both proteins are required for formation of a complex with tightly held Ca^{2+}, and complex formation hinders the tendency of PDP1c to form a dimer.

Mammalian pyruvate dehydrogenase complex (PDC)[1] catalyzes the irreversible conversion of pyruvate to acetyl-CoA along with the reduction of NAD^+ via sequential steps catalyzed by the pyruvate dehydrogenase (E1), dihydrolipoyl acetyltransferase (E2), and dihydrolipoyl dehydrogenase (E3) components (*1*). PDC is tightly regulated by a phosphorylation−dephosphorylation cycle that determines the proportion of active (nonphosphorylated) E1 (*1*−*3*). PDC inactivation of E1 is carried out by pyruvate dehydrogenase kinase (PDK) isoforms (*3*−*6*) and reactivation by pyruvate dehydrogenase phosphatase (PDP) isoforms (*3*, *7*, *8*). There are four known PDK isoforms and two known PDP isoforms. In Ca^{2+}-sensitive tissues, pyruvate dehydrogenase phosphatase isoform 1 (PDP1) is the prevailing phosphatase isoform (*8*). PDP1 catalyzes a Mg^{2+}-requiring, Ca^{2+}-stimulated dephosphorylation of phosphorylated E1 (P-E1) (*3*, *9*, *10*). At standard levels of P-E1, PDP1 activity is enhanced manyfold when P-E1 and PDP1 are both bound by E2 (*12*), which forms the core of the complex. Indeed, Ca^{2+} stimulation involves Ca^{2+}-aided binding of PDP1 to E2 (*12*−*15*).

PDP1 is composed of two subunits (*13*, *14*). Its catalytic subunit, PDP1c (M_r = 52.6 kDa), is in the phosphatase 2C class (*7*); however, the sequence of PDP1c is only ~21% identical with that of cytosolic protein phosphatase 2C α and β isoforms (*7*). The regulatory subunit, PDP1r (M_r = 96 kDa), is a flavoprotein with a bound FAD (*14*); the sequence of PDP1r (*16*) is distantly related to the other large flavoproteins found in bacteria[2] and mammalian mitochondria [dimethylglycine dehydrogenase (*16*) and sarcosine dehydrogenase[2]]. PDP1r plays a regulatory role in which it increases the concentration of Mg^{2+} required for efficient PDP1c catalysis (*17*). Spermine and to a lesser degree other polyamines reduce the K_m of PDP1 for Mg^{2+} (*18*) to a level similar to that of PDP1c alone (*7*, *8*). That apparently occurs by binding of spermine to PDP1r (*17*).

† This work was supported by National Institutes of Health Grant DK18320. This work was also supported by the Agricultural Experiment Station (Contribution 04-387-J).

* To whom correspondence should be addressed: Department of Biochemistry, Kansas State University, Willard Hall, Manhattan, KS 66506. Phone: (785) 532-6116. Fax: (785) 532-7278. E-mail: bchter@ksu.edu.

‡ Present address: Department of Chemistry, Gebze Institute of Technology, P.B. 141 Gebze/Kocaeli, Turkey 41400.

[1] Abbreviations: PDC, pyruvate dehydrogenase complex; E1, pyruvate dehydrogenase component; P-E1, phosphorylated E1; E2, dihydrolipoyl acetyltransferase component; L1 domain, NH_2-lipoyl domain of E2; L2 domain, interior lipoyl domain of E2; PDP1, pyruvate dehydrogenase phosphatase isoform 1; PDP1c, catalytic subunit of PDP1; PDP1r, FAD-containing, regulatory subunit of PDP1; PDP2, pyruvate dehydrogenase phosphatase isoform 2; E3, dihydrolipoyl dehydrogenase; E3BP, E3-binding protein; PDK, pyruvate dehydrogenase kinase; GST, glutathione *S*-transferase; SDS, sodium dodecyl sulfate; PAGE, polyacrylamide gel electrophoresis; ITC, isothermal titration calorimetry; ASI, aligned sequence identity; AUC, analytical ultracentrifugation; apparent K_{act}, concentration giving half-maximal activation.

10.1021/bi048901y CCC: $27.50
Published on Web 11/05/2004

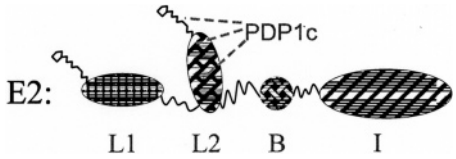

FIGURE 1: Interaction of PDP1c with the L2 domain of E2. The domain structure of E2 includes the two lipoyl domains, L1 and L2, an E1 binding domain (B), and an oligomer forming the inner (I) domain. These domains are connected by mobile linker regions that are high in proline. PDP1 or, more specifically, PDP1c binds to the L2 domain by an interaction that requires a specific structure of the lipoyl prosthetic group and in the lipoyl domain both near the lipoyl group and at the other end of the domain (indicated with dashed lines) (*15*, *26*).

E2 consists of four independently folded domains (Figure 1) connected to each other by mobile linker regions 20−30 amino acids in length (*2*, *3*, *19*). First, there are two ~10 kDa lipoyl domains, an NH_2-terminal one (L1) and an interior one (L2). Then there is an E1 binding domain and finally the assembly-forming, acetyltransferase-catalyzing C-terminal domain. When mammalian E2 subunits are expressed alone, association of 20 trimer units of E2's C-terminal domain produces a central cavity in the shape of a dodecahedron (*20*). When E2 is expressed along with the E3 binding protein (E3BP), a limited number of C-terminal domains of this protein substitute in the dodecahedron structure (*21*). Outside this assembled inner core, 20−30 E1 tetramers ($\alpha_2\beta_2$) are typically bound in preparations of the complex (*1*−*3*), although the E2 60mer has a capacity for binding ~60 E1 tetramers and the E2·E3BP subcomplex has a capacity to bind ~48 E1 tetramers (*21*). Beyond E3BP's C-terminal domain that contributes to the inner core, linker regions connect first to an E3 binding domain and then to an N-terminal lipoyl domain (*22*−*24*).

Just PDP1c, alone, undergoes Ca^{2+}-dependent binding and activation (*7*) via an association with the L2 domain of E2 (Figure 1) (*15*). Neither PDP1 nor PDP1c interacts productively with the L1 domain of E2 or with the lipoyl domain of E3BP, and their binding to L2 requires the lipoyl group (*15*, *25*, *26*). Ca^{2+}-aided binding to the gel-anchored GST−L2 protein has been used to selectively purify PDP1 (*15*) and PDP1c (*26*, *27*). The surface of the L2 structure that contributes to binding PDP1 and PDP1c has been mapped by comparing the capacities of mutant or lipoyl analogue substituted L2 domains to competitively interfere with E2 activation (*26*). Two regions were found to be important. One region includes a set of residues near the lipoyl group and the octanoyl but not the dithiolane ring structure of the lipoyl group. At the other end of the lipoyl domain, a cluster of glutamates (residues 162, 179, and 182) along with Gln181 made a critical contribution to binding PDP1 and PDP1c.

At saturating Mg^{2+} concentrations, the major means by which Ca^{2+}-facilitated association of PDP1 with E2 enhances PDP1 activity is by providing greatly enhanced access to E2-bound P-E1. Specifically, there are large decreases in the apparent K_m values for P-E1 when P-E1 is bound along with PDP1 or PDP1c to E2 (*12*, *17*). In the absence of E2, P-E1 levels required to saturate PDP1 activity are approached only when the P-E1 concentration is more than 1 order of magnitude greater than the highest intramitochondrial level of E1 (≤ 10 μM within the matrix space of heart mitochondria). Besides this large effect on activity, Ca^{2+}-dependent binding to E2 causes some decrease with both PDP1 and PDP1c in the K_m for Mg^{2+} (*17*, *28*).

Past studies with EGTA-Ca buffers indicated that near-micromolar levels of Ca^{2+} supported E2 activation of PDP1 (*10*, *29*). This has not been evaluated with PDP1c. Mutation of Asp173 in bovine PDP1c was found to interfere with Ca^{2+}-dependent activation by E2. It was suggested that this residue was part of an EF-hand (*7*, *11*). However, this is in a part of the sequence that is completely conserved in PDP2 (*8*); PDP2 does not undergo Ca^{2+}-dependent activation or bind to E2 (*8*, *30*). Advanced studies on the structure of PDP1c[3] have established the folding of most of the backbone of PDP1c and demonstrate that Asp173 is not part of an EF-hand. Indeed, the sequences and structures of PDP1c (*7*)[3] and the L2 domain (*19*, *31*) indicate that these structures lack domains that normally participate in tightly binding Ca^{2+} (EF-hand or C_2 domains). These observations point to the existence of a distinct means of high-affinity binding of Ca^{2+} in the PDP1c·Ca^{2+}·L2 complex. One study suggested that PDP1 directly binds Ca^{2+} and that a second site is created when PDP1 binds to E2 (*14*). Here, we assess the protein requirements for creating a high-affinity Ca^{2+} binding site in studies with PDP1c and the L2 domain. These studies not only reveal an atypical dual protein requirement but also uncover an unexpected PDP1c oligomeric state and change in that state upon Ca^{2+}-dependent binding to L2. We further evaluated how Mg^{2+} and the regulatory subunit, PDP1r, affect the Ca^{2+} levels required both for binding of PDP1c to the L2 domain and for supporting E2-enhanced phosphatase activity. We also evaluate the capacity of the E2 60mer to bind PDP1c molecules.

EXPERIMENTAL PROCEDURES

Materials. Bovine PDC, bovine E1, and ^{32}P-labeled phosphorylated PDC and E1 were prepared as previously described (*13*, *15*, *29*). The GST−L2 protein was prepared as previously described (*32*). Human E2 and E2·E3BP were purified as described previously (ref *21*, Supplement). The preparation of human E1 will be described elsewhere.[4] ^{32}P-labeled phosphate was introduced into human E1 using human PDK2. In all preparations of phosphorylated proteins, [γ-^{32}P]ATP was hydrolyzed by treatment with hexokinase/

[2] The sequence of bovine PDP1r shows the highest full-length aligned sequence identity (ASI) with bacterial proteins whose role has not been established [ASI of 39% with Q92uw2_Bac, a putative dehydrogenase from *Rhizobium meliloti*; ASI of 36.5% with pSDH_Bac1 (NP_102909), a putative sarcosine dehydrogenase from *Rhizobium loti*] and is clearly related to mitochondrial sarcosine dehydrogenase (ASI of 33% with human sarcosine dehydrogenase) and dimethylglycine dehydrogenase (ASI of 30.9% with the human enzyme). In these proteins, the N-terminal end of PDP1r aligns with an FAD-containing domain and the C-terminal end aligns with a tetrahydrofolate binding domain. There are separate proteins that align with each of these domains. The N-terminal domain aligns with members of the so-called D-amino acid oxidase family (gnl/CDD/7951 pfam01266) of FAD-dependent oxidoreductases such as glycerol-3-phosphate dehydrogenase, sarcosine dehydrogenase, D-alanine dehydrogenase, and D-aspartate oxidase. The C-terminal end aligns with members of the glycine cleavage T-protein family (gnl/CDD/8063 pfam 01571).

[3] S. R. Ernst, L. J. Reed, D. W. Carroll, D. B. McCarthy, A. Turkan, T. E. Roche, and M. L. Hackert, unpublished results.

[4] Y. Hiromasa, H. Bao, X. Yan, X. Gong, A. Yakhnin, J. Dong, S. A. Kasten, L. Hu, T. Peng, J. C. Baker, M. Sadler, and T. E. Roche, manuscript in preparation.

glucose followed by exhaustive dialysis to remove ADP, glucose, and Mg^{2+}. Homogeneous PDP1 was prepared by affinity chromatography by Ca^{2+}-dependent binding to the GST−L2 protein anchored on GSH−Sepharose followed by elution with EGTA (*15*). Most activity studies were conducted with bovine PDP1 purified only through the DEAE column step (*13*) since PDP1 remains more stable than the highly purified PDP1. PDP1c was expressed in *Escherichia coli*, and homogeneous PDP1c was prepared as previously described using affinity chromatography with the GST−L2 protein (*26*, *27*).

Phosphatase Activity. PDP1 and PDP1c were assayed as previously described (*13*, *15*, *26*) using both a spectrophotometric assay that measures recovery of PDC activity or a dephosphorylation assay that measures the amount of ^{32}P-labeled phosphate released from E1 using phosphorylated PDC or free phosphorylated E1 as a substrate. In routine assays, final reaction mixtures also contained 50 mM MOPS-K (pH 7.4), 0.1 mM EDTA, 1.2 mM Ca^{2+}, 1.0 mM EGTA, 0.4 mg/mL BSA, 2 mg/mL Pluronic F68, 20 μg of phosphorylated PDC, and 0.02−0.03 unit of PDP activity in a final reaction volume of 25 μL (1 unit = 1 nmol of ^{32}P-labeled phosphate released per minute using ^{32}P-phosphorylated PDC as a substrate). Reactions were normally initiated by addition of $MgCl_2$ at the indicated concentration (10 mM for maximal activities) and allowed to proceed for 2 min followed by removal of either 20 μL to a cuvette (spectrophotometric assay of PDC reactivation) or 200 μL of 10% trichloroacetic acid with immediate vortex mixing (assay of ^{32}P-labeled phosphate released). In the latter assay, after incubation for at least 30 min on ice and centrifugation to pellet precipitated protein, 90 μL was withdrawn and the amount of ^{32}P-labeled phosphate measured in the supernatant.

EGTA-Ca Buffers. Initially, 100 mM EGTA and 100 mM $CaCl_2$ stock solutions were prepared, and concentrations of both were evaluated using a Ca^{2+}-selective electrode and a Ca^{2+} standard solution. Calculated proportions were added to 110 mM Hepes buffer containing 2 mg/mL Pluronic F68, 2 mg/mL BSA, and 2 mM DTT to give 5 mM EGTA and the desired free concentration of Ca^{2+} ion in a final volume of 10 mL; 5 μL of this buffer was used in an assay volume of 25 μL (final pH of 7.2). Concentrations of free Ca^{2+} in the presence of 1 mM EGTA, 0.1 mM EDTA, 10 mM Mg^{2+}, or 0.8 mM Mg^{2+} at pH 7.2 were computed using an iterative computer program kindly provided by I. Udovichenko (University of California, San Diego, CA). In a pH-sensitive manner, the program calculates the amount of free Ca^{2+} based on the simultaneous EGTA and EDTA equilibrium binding of Ca^{2+} and Mg^{2+}. The program is a functional improvement over ones that this laboratory previously utilized for calculating EGTA-Ca buffers (*29*, *33*), but it uses the same constants, as described by Portezehl et al. (*34*), and gives the same results. Atomic flame absorption spectroscopy was used to measure the trace level of Ca^{2+} in the other buffer components. For instance, when 10 mM $MgCl_2$ was used, this was found to be 20 ± 2 μM; these values were included with the added Ca^{2+} in the calculating the level of free Ca^{2+}. PDP activity was monitored in the presence of EGTA-Ca buffers by the ^{32}P-labeled phosphate release assay.

Binding Studies Using Affinity Retardation Chromatography. Mini columns were prepared by mixing 2 mg of the GST−L2 protein with 3 mL of GSH−Sepharose and making a column for a set of comparisons with a bed volume of ~0.6 mL. The column elution volume was measured more precisely when a symmetric elution of PDP activity was observed (one case), and the binding affinity was then analyzed using a quantitative affinity retardation chromatography analysis (*45*).[5] Columns were all equilibrated with 20 mM Hepes-Cl (pH 7.2), 1 mg/mL BSA, and 2 mg/mL Pluronic F68. In addition, the buffer contained either 1 mM EGTA or an EGTA-Ca buffer to keep free Ca^{2+} at a specific level and either 0.8 or 10 mM Mg^{2+}. Two to ten units of PDP1 or PDP1c was applied to a column and eluted at ~20 μL/min with the buffer described above containing the desired concentration of Ca^{2+}. In reference runs, fractionation was performed with 1 mM EGTA with no added Ca^{2+} and Mg^{2+} (prevents PDP1 or PDP1c binding), and after passage of 2−4 column volumes with the other buffer conditions, this EGTA-buffer was used to elute any residual PDP1 or PDP1c that was still bound to a column. The volume of fractions was measured (~60 μL), and each fraction was assayed for the phosphatase activity in duplicate by the spectrophotometric assay. As needed, additional Ca^{2+} was introduced into activity assays to compensate for EGTA introduced from a fraction.

Sedimentation Velocity and Sedimentation Equilibrium Studies on PDP1c and PDP1c with L2. Sedimentation velocity studies were conducted with different levels of PDP1c and PDP1c with the L2 domain using a Beckman XL-I analytical ultracentrifuge (AUC) with a four-position AN-60Ti rotor and double-sector 1.2 cm cell(s) with a charcoal-filled Epon (40 000 rpm) or aluminum (55 000 rpm) centerpiece using procedures previously described (*21*, *35*). Sedimentation was monitored using absorbance optics. After equilibration at 20 °C and 3000 rpm, initial scans were taken and then the rotor speed was increased to 40 000 or 55 000 rpm. Radial scans were then taken at 4−8 min intervals with the detection by the absorbance mode at the indicated wavelength. On the basis of the amino acid composition, the extinction coefficients at 280 nm are 50 450 M^{-1} cm^{-1} for PDP1c and 9650 M^{-1} cm^{-1} for L2 (*36*); these values agreed well with estimates using BCA protein measurement.

[5] Affinity retardation chromatography (ARC) has been used to determine binding constants for weak protein−protein interactions (*46*). In the ARC method, one of the interacting proteins is immobilized in a column at a level *A* and an interacting protein is passed through at a concentration *B*. A rapid binding equilibrium relative to the flow rate is assumed (requires, below, that $f < 1.00$). Then, the difference in the elution volumes of the mobile protein in the presence and absence of the immobilized protein is directly related to the binding constant of interacting proteins (*46*). $K_{av} = (V_e - V_0)/(V_t - V_0) = (3V_e/2V_t) - {}^1/_2$, $K_{avARC} = [3V_e(1 + f)]/2V_t - {}^1/_2$, and $\Delta K_{av} = K_{avARC} - K_{av}$, where V_e is the unretarded elution volume, V_{eARC} is the retarded elution volume, V_0 is the void volume ($V_t/3$), V_t is the column volume, and $f = (V_{eARC} - V_e)/V_e$. Therefore, $V_{eARC} = V_e(1 + f)$, and from algebraic derivation, $f = 2V_t\Delta K_{av}/3V_e$ and $K_d = [A - (A + B)f + Bf^2]/f$, where ab = Bf, $a = A - ab = A - Bf$, and $b = B - ab = B - Bf$, where *a*, *b*, and ab are the concentrations of free (but immobilized) A, free B, and the complex, respectively. Using these equations, $\Delta K_{av} = 0.887$, $f = 0.935$, and $K_d = 1.29$ μM for the GST·L2·Ca^{2+}·PDP complex at saturating Ca^{2+} concentrations in the absence of added Mg^{2+}. It should be noted that when $A \gg B$ as in our studies, the concentration of B (and its changing concentration during the pass through the column) has a minimal effect on V_{eARC} (*46*). The experimental error on each fraction was ±0.5 μL, and the column (490 μL) and void (163 μL) volumes were independently measured (±5 μL). The overall experimental error for the estimated K_d should be less than ±15%.

Extinction coefficients at other wavelengths were determined by the ratio of the absorbance at that wavelength to the absorbance of the protein at 280 nm as determined from variable-wavelength scans.

Sedimentation profiles including a consecutive set of at least four scans were analyzed to obtain the apparent distribution of sedimentation coefficient $g(s^*)$ using DCDT+ version 1.16 provided by J. S. Philo (www.jphilo.mailway-.com) (*37*, *38*). Buffer density and viscosity were calculated with Sednterp version 1.08 (www.jphilo.mailway.com). The partial specific volumes of PDP1c (0.734 mL/g at 20 °C, 0.725 mg/g at 4 °C) and other components (*21*, *35*) were calculated from their amino acid composition using Sednterp. The apparent sedimentation coefficient distribution function $g(s^*)$ versus s^* provides a useful boundary shape for evaluating associating systems (*37*−*40*). All of the software used in these analyses are available from the RASMB site (www.asmb.bbri.org/RASMB/rasmb.html); some have been updated to later versions.

Sedimentation of PDP1c was evaluated with 0.38, 0.76, 1.9, 3.8, 9.5. 19.0, and 38.0 μM PDP1c in the presence and absence (with EGTA) of Ca^{2+}. The S value change with concentration was fit by a monomer−dimer equilibrium using the following analyses. The S value of the dimer was estimated from extrapolation of the near-linear phases at high concentrations of $1/S$ versus $1/C$ plot (*41*). The S value of the monomer was estimated from extrapolation of the near-linear change in a plot of S versus C as the lowest concentrations. The scans were fit to a monomer−dimer equilibrium model model using SEDFIT version 8.8c and SEDPHAT version 2.0b developed by P. Schuck (www.biochem.uthscsa.edu/auc/software) (*42*, *43*). SEDPHAT was also used to perform a global fit on the set of sedimentation velocity profiles. Apparent K_d values were derived from the individual fit using SEDFIT and SEDPHAT for each PDP1c level, from the average of those values, and from the global fit using all levels by SEDPHAT. The error ranges for K_d values were based on the F statistic 95% confidence interval calculated by these programs. The $g(s^*)$ profiles generated from the SEDFIT monomer−dimer model were also compared to the $g(s^*)$ profiles from the sedimentation runs. The various $g(s^*)$ profiles at different PDP1c levels were also simulated by a monomer−dimer model using SedAnal version 3.61 with variation in the apparent K_d (*37*−*39*). For the $2M \rightleftarrows D$ equilibrium, the following equations apply. $K_d = C_m^2/C_d$, where C_m and C_d are the concentration of the monomer and dimer, respectively; the total concentration as monomer $C_o = C_m + 2C_d$. $K_d = (C_m/M_m)^2/(C_d/2M_m) = 2(C_m)^2/M_mC_d$ and is expressed in fractions of monomer $K_d = 2C_o(f_m)^2/M_m(1 - f_m)$, where f_m is the fraction of monomer. M_w (the weight average molecular mass) $= f_mM_m + f_dM_d$, and $f_m = 2 - M_w/M_m$. The mass of the monomer, M_m, based on the amino acid sequence is 52 625 Da.

Sedimentation equilibrium studies on PDP1c were conducted using a charcoal-filled Epon centerpiece with six-sector cells. Normally, 50 μL samples were overlayed over 20 μL Fluorinert FC-43 silicon oil (3M Industrial Chemical Products Division), and 100 μL of matched solvent was introduced in the reference position. PDP1c was evaluated at three concentrations, and an equilibrium was attained at multiple rotor speeds. PDP1c at 0.15, 0.30, and 0.45 mg/mL was equilibrated at 8000, 10 000, 14 000, and 17 000 rpm at 4 °C. Following equilibration at the lowest speed during the 30 h period, an equilibration time of at least 8 h was used for the transition to a higher speed. The stability of the established concentration gradient was confirmed over a period of at least 4 h before final measurements were taken.

Sedimentation equilibrium data for PDP1c were fit both individually and by a global weighted fit using a monomer−dimer model and a monomer−trimer model using Beckman software (version 4.0) that was provided with the Optima XL-I ultracentrifuge. Selected results demonstrating the fit from the monomer−dimer global analysis are shown.

Sedimentation Velocity Analysis of Binding of PDP1c to the E2 60mer. Binding of PDP1c to E2 was evaluated in samples containing 0.1085 μM E2 60mer alone and with 1.9, 3.8, 5.7, 9.5, and 19 μM PDP1c and each of these PDP1c levels alone in a buffer containing 4 mM $MgCl_2$, 0.2 mM free Ca^{2+} (0.7 mM Ca^{2+} and 0.5 mM EGTA) in 30 mM Tris-HCl (pH 7.4), and 50 mM NaCl. Centrifugation of 350 μL samples and matched solvent at 20 000 rpm and 20 °C was monitored at 280 nm by scans at 6 min intervals. The analyses used to estimate the extent of binding of PDP1c to E2 were essentially the same as those employed to estimate the extent of binding of PDK2 (*35*) and E1 (*21*) to E2. Succinctly, the extent of binding was based on the decrease in the level of trailing PDP1c and the increase in the absorbance beyond E2 in the leading peak, and by comparing the increase over E2 absorbance (converted to concentration) in the integrated $g(s^*)$ peaks. Each method gave similar results. Results from the estimates of bound PDP1c using the integrated $g(s^*)$ peaks are plotted. On the basis of the protein level determined using interference optics and simultaneous measurements at 280 nm at the lower protein concentrations, the extinction coefficient of E2 at 280 nm is 42 925 M^{-1} cm^{-1} per E2 subunit (*21*, *35*).

Isothermal Titration Calorimetry (ITC). Titrations were performed using a MicroCal MCS titration calorimeter (MicroCal, Inc., Northhampton, MA) at 30 °C (*44*, *45*). Concentrated PDP1c and L2 samples were dialyzed against Chelex-100-treated 30 mM Tris buffer containing 30 mM NaCl (final pH of 7.3). The initial solution in this buffer, with proteins added as indicated, was introduced to fill the 1.32 mL sample cell. The reference cell contained deionized water alone. All solutions were degassed under vacuum for ∼10 min before ITC experiments. After equilibration at 30 °C, an appropriate concentration of ligand (Ca^{2+} or L2, typically 25−50 times higher than the desired final concentration) was added in the same buffer at discrete intervals. The observed heat change was measured after each injection. The total observed heat change was corrected for the heat of dilution of the ligand by performing control titrations in the absence of protein. Origin software provided by MicroCal was used to integrate the calorimetric output curves; this includes corrections for the volume displaced from the cell and small effects of dilution of the macromolecules in the cell with consecutive injections of the concentrated ligand. Because the output indicated multiple equilibria were involved (see the Results and Discussion), the integrated titration curves could not be fit to give apparent binding constants.

$^{45}Ca^{2+}$ Binding with L2 and PDP1c Using Centrifugal Filtration Device. Samples were incubated in 20 mM Hepes-K, 60 mM KCl (pH 7.2), and 5 mM $MgCl_2$. $^{45}CaCl_2$ was

added at concentrations of 5−50 μM. Variables were inclusion of no protein, 10 μM PDP1c, 30 μM L2, or both. The tubes containing these mixtures were incubated at room temperature for ~2 h, and 10 μL aliquots (duplicate) were transferred into 10 mL of scintillation cocktail; these initial samples had a radio specific activity of 607 ± 3 cpm/pmol. The remaining 180 μL mixtures were transferred into Microcon-YM10 filter devices which had been prerinsed with buffer [20 mM Hepes-K, 60 mM KCl (pH 7.2), and 5 mM $MgCl_2$]. The tubes were centrifuged at 3000 rpm. Filtrates and retentates were saved, and the radioactivity was determined; the volumes of retentates were measured in duplicate. The retentate volumes were ≥140 μL.

RESULTS AND DISCUSSION

Effect of Ca^{2+} on the Activities of PDP1 and PDP1c at Different Levels of Mg^{2+}. The changes in activity of PDP1 (Figure 2A) and PDP1c (Figure 2B) were evaluated with variation in free Ca^{2+} ions (using EGTA-Ca^{2+} buffers) at saturating (10 mM) and subsaturating (0.8 mM added) Mg^{2+} concentrations. With 0.8 mM Mg^{2+} added, the calculated concentration of free Mg^{2+} varies from 0.6 to ~0.8 mM as the free Ca^{2+} level increases. For the sake of simplicity, we only indicate the added Mg^{2+} level throughout. Ca^{2+} activated PDP1 with a half-maximal increase (apparent K_{act}) at ~1.0 and ~3.0 μM at the saturating and subsaturating Mg^{2+} concentrations, respectively. With PDP1c, the half-maximal increase in activity occurred at ~3.0 μM free Ca^{2+} in the presence of either 10 or 0.8 mM Mg^{2+}. The lower apparent K_{act} of PDP1 at the saturating Mg^{2+} concentration suggests that the PDP1r subunit fosters a Mg^{2+}-dependent increase in the affinity of PDP1 for Ca^{2+}.

Both PDP1 and PDP1c activities rose more steeply with an increase in Ca^{2+} concentration at the lower Mg^{2+} concentrations (Figure 2A,B). The more gradual response at 10 mM Mg^{2+} may be due to Mg^{2+} competitively interfering with Ca^{2+} binding. Still with 10 mM Mg^{2+}, maximal activity was reached at 20 μM Ca^{2+} with PDP1 (due to the lower apparent K_{act}) but required 100 μM Ca^{2+} for PDP1c (Figure 2A,B). With 10 mM Mg^{2+} and <0.5 μM free Ca^{2+}, PDP1 and PDP1c exhibited ~17 and ~10% of the maximal activity, respectively. It is uncertain whether, in the absence of Ca^{2+}, Mg^{2+} ions have any capacity to substitute productively for Ca^{2+} ions. If that is the case, Mg^{2+} must do so with a much weaker binding affinity and a greatly reduced capacity to activate.

The drop in phosphatase activity at high Ca^{2+} levels may result from Ca^{2+} competing with Mg^{2+} ions at the active site. The sharper drop in the PDP1c level at lower Mg^{2+} concentrations (35% decrease) than at the higher Mg^{2+} concentrations (7.5% drop) fits this interpretation (Figure 2B). However, a similar trend is not apparent with PDP1 (Figure 2A).

Binding of PDP1 and PDP1c to the GST−L2 Protein as the Ca^{2+} Concentration Is Varied in the Presence and Absence of Mg^{2+}. Figure 3A shows the profiles for elution of PDP1 at 0.34, 0.68, and 1.4 μM free Ca^{2+} levels in the presence of 10 mM Mg^{2+}. The reference elution profile was obtained with buffer containing 1 mM EGTA alone. With increasing Ca^{2+} concentrations, PDP1 was retarded more in the column and tailing occurred. At free Ca^{2+} concentrations

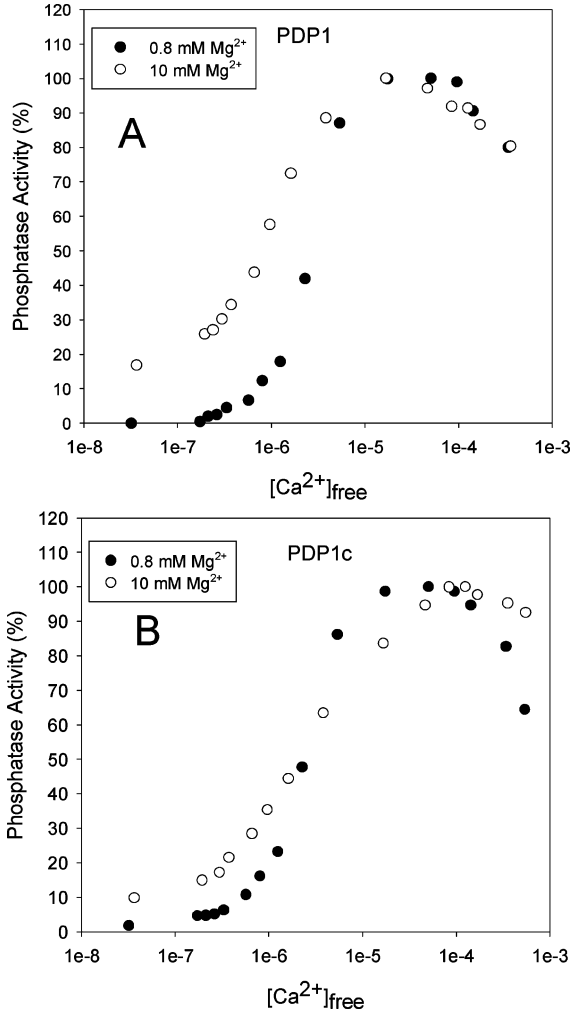

FIGURE 2: Effects of variation in the Ca^{2+} concentration on PDP1 (A) and PDP1c (B) activity at saturating (10 mM) and subsaturating (0.8 mM) concentrations of Mg^{2+}. Using EGTA-Ca^{2+} buffers to control the free Ca^{2+} level, phosphatase activity was assessed in duplicate by measuring the amount of ^{32}P-labeled phosphate released from P-PDC as described in Experimental Procedures. In panel A, the maxima (100% activities) were 197 and 484 nmol min^{-1} mg^{-1} at 0.8 and 10 mM Mg^{2+}, respectively; on the basis of staining with Coomassie R-250 following SDS−PAGE analysis, PDP1 constituted ~40% of the protein in the DEAE fraction that was used as a source of PDP1. In panel B, the maximum (100%) velocities for homogeneous PDP1c activity were 745 and 1405 nmol min^{-1} mg^{-1} at 0.8 and 10 mM Mg^{2+}, respectively.

of ≥3 μM and using fairly slow flow rates (~20 μL/min), PDP1 was completely bound to the GST−L2 column and was selectively eluted with 1 mM EGTA alone [data not shown; this condition is similar to that used for affinity purification of PDP1 (*15*)]. Because of the tailing, we are not able to use unambiguously the observed elution profiles to calculate Ca^{2+}-dependent equilibrium constants for formation of the PDP1·GST−L2 complex by the affinity interaction chromatography technique since that requires rapid reversible binding relative to the flow rate (*46*). Nevertheless, the results indicate that in the presence of 10 mM Mg^{2+}, PDP1 binds tightly to the GST−L2 protein at low micromolar levels of Ca^{2+}. Therefore, there is a strong correlation between the binding interaction and the level of Ca^{2+} required to support activity. Equilibrium binding studies evaluating $^{45}Ca^{2+}$ binding (ref *14* and data herein) indicate that higher levels of Ca^{2+} are required. To some extent, that is probably

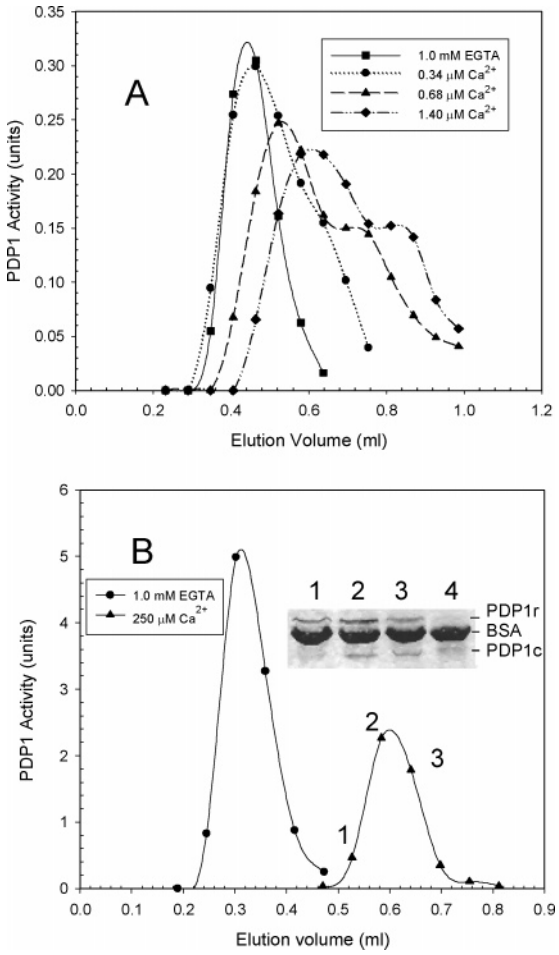

FIGURE 3: Binding of PDP1 to and elution from GSH−Sepharose−GST−L2 at varied Ca^{2+} levels in the presence of 10 mM Mg^{2+} (A) and at saturating Ca^{2+} levels in the absence of Mg^{2+} (B). In panel A, elution profiles are shown for PDP1 activity in the presence of 10 mM Mg^{2+} when the free Ca^{2+} concentration was maintained at the indicated levels by EGTA-Ca buffers or <0.01 μM with 1.0 mM EGTA. In the case of EGTA alone, half as many units were loaded as in the other profiles. In panel B, the main figure shows profiles for the elution of PDP1 activity from a GSH−Sepharose−GST−L2 mini column (bed volume of 600 μL with 56 μL fractions collected) using buffers lacking Mg^{2+} with either no free Ca^{2+} (1.0 mM EGTA) or 250 μM Ca^{2+} (1.0 mM EGTA and 1.25 mM Ca^{2+}). The inset in panel B shows an SDS−PAGE pattern for selected fractions from the elution with 250 μM Ca^{2+}. Fractions 1−3 used in SDS−PAGE are identified; fraction 4 was the column volume fraction (not shown in the elution profile) following a change to elution with 1.0 mM EGTA buffer to remove free Ca^{2+}. For both panels, the preparation and elution from the mini columns and PDP1 activity measurements (in the PDC activation assay, 1 unit equals an increase in PDC activity of 1 μmol of NADH per minute) were performed as described in Experimental Procedures.

due to nonspecific binding of the labeled Ca^{2+} causing the free Ca^{2+} concentration to be less than the concentration of added Ca^{2+} when low Ca^{2+} concentrations are not maintained by using EGTA-Ca buffers.

With no added Mg^{2+}, even at a saturating level of free Ca^{2+} (250 μM), PDP1 was bound with a weaker affinity by the gel-bound GST−L2 protein (Figure 3B). With EGTA included, PDP1 eluted at a reference elution volume of 310 μL, but with 250 μM Ca^{2+} included, PDP1 eluted at a retarded volume of 600 μL. This is a sufficiently well-behaved elution profile for estimating a binding constant (K_d = 1.3 ± 0.2 μM) by affinity retardation chromatography analysis (*46*).[5] However, a small portion of the phosphatase activity still trailed, and a small amount eluted only when EGTA was passed through the column. The inset in Figure 3B shows an SDS−PAGE analysis of selected fractions. These GST−L2 binding studies were all conducted with 1.0 mg/mL BSA (major band migrating between PDP1r and PDP1c, Figure 3B inset). With 250 μM Ca^{2+} and no Mg^{2+}, a portion of PDP1r dissociated from PDP1c, and since this PDP1r was no longer retarded by interaction with the GST−L2 protein, it eluted prior to most of the PDP1 (fraction 1, lane 1, Figure 3B inset). Lane 2 (fraction 2) shows the normal relative intensity of staining for a 1:1 ratio of the PDP1r and PDP1c subunits. Lane 3 from the backside of the with Ca^{2+} peak in Figure 3B shows an increase in the level of PDP1c relative to the level of PDP1r. Primarily, PDP1c was eluted when EGTA was subsequently passed through the column (lane 4, Figure 3B, inset). Inclusion of Mg^{2+} not only enhanced binding of PDP1 to the GST−L2 protein (above) but also hindered dissociation of PDP1r from PDP1c. The PDP1c:PDP1r ratios appeared to be constant in SDS−PAGE analyses (data not shown), including the tailing fractions in Figure 3A. Inclusion of subsaturating Mg^{2+} concentrations led to results intermediate between those in the absence of Mg^{2+} and those with saturating Mg^{2+} concentrations but gave overly tight binding and asymmetric peaks at higher Ca^{2+} levels to allow K_d values to be estimated, but the K_d was judged to be <1 μM based on the above estimate of 1.3 μM in the absence of Mg^{2+}.

Similar binding experiments were conducted with recombinant PDP1c. Again, PDP1c eluted rapidly in the presence of EGTA. With >10 μM Ca^{2+}, nearly all the PDP1c remained bound to the column until EGTA was added. With 1.4 μM free Ca^{2+} and 10 mM Mg^{2+}, some PDP1c slowly eluted, but even after 3 column volumes had been collected, nearly half of the PDP1c activity was still eluted when 1.0 mM EGTA was passed through the mini column. Unlike PDP1, in the absence of added Mg^{2+}, PDP1c was fully bound to the GST−L2 affinity column at saturating Ca^{2+} concentrations (250 μM) and, after 3 column volumes, was again mostly eluted by 1.0 mM EGTA. Therefore, PDP1c binds tighter to the gel-bound GST−L2 protein than PDP1 with a particularly large difference in binding affinities when compared in the absence of added Mg^{2+}. Apparently, the PDP1r subunit not only increases the K_m of PDP1 for Mg^{2+} but also causes the Ca^{2+}-dependent binding of PDP1c to L2 to be strengthened at higher Mg^{2+} levels.

Determination of the Oligomeric State of PDP1c by Analytical Ultracentrifugation Studies. PDP1 is known to be a heterodimer (*13*, *14*), but the oligomeric state of PDP1c has not been described. The rate of sedimentation of PDP1c increased with concentration, indicating that a rapid equilibrium was being maintained between two or more oligomeric states. Figure 4 shows how the $g(s^*)$ profiles shift to higher S ranges with increasing PDP1c concentrations in the presence of Ca^{2+} (0.2 mM). Sedimentation was followed at the wavelengths given in the Figure 4 legend; the overlay shows profiles normalized to their relative absorbance values at 280 nm. The peak in the $g(s^*)$ profile shifted from 3.44 S at the lowest concentration (0.38 μM) to 4.84 S at the highest level (38 μM). The vertical lines (Figure 4) indicate the S values estimated for the monomer and dimer using the extrapolations described in Experimental Procedures. There

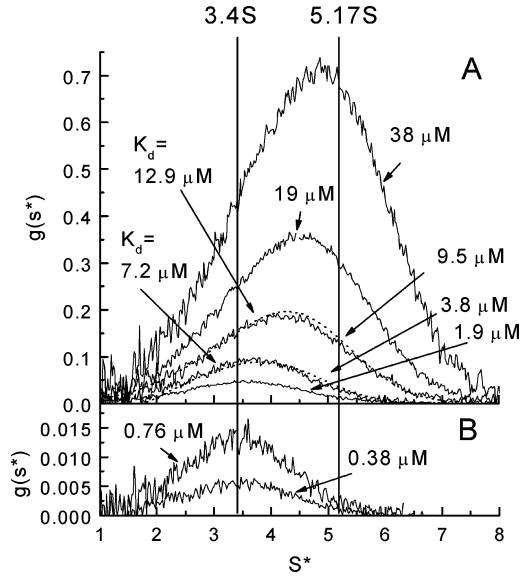

FIGURE 4: Sedimentation velocity profiles for different levels of PDP1c in the presence of 0.2 mM free Ca^{2+}. The panels show $g(s^*)$ profiles from sedimentation velocity profiles that have been normalized on the basis of the relative absorbance (measured or calculated) at 280 nm. Sedimentation at 40 000 rpm and 20 °C was monitored at 220 nm for 0.38, 0.76, and 1.9 μM PDP1c, at 234 nm for 3.8 μM PDP1c, at 280 nm for 9.5 and 19 μM PDP1c, and at 290 nm for 38 μM PDP1c. The dashed lines for the profiles at 3.8 and 9.5 μM show $g(s^*)$ profiles generated from the fit of the initial scans using SEDFIT and a monomer−dimer model. The fits used the S values estimated by extrapolation (see Experimental Procedures) for the monomer (3.4 S) and the dimer (5.17 S) (solid vertical lines). As examples of individual fits using the monomer−dimer equilibrium, SEDFIT modeling of the profiles obtained with 19 and 38 μM PDP1c yielded K_d values (error ranges) of 10.95 (9.8−12.0 μM) and 8.6 μM (6.5−9.9 μM), respectively; with results from additional concentrations (9.5 and 3.8 μM) included, an average K_d of 9.9 ± 2.5 μM was estimated.

was no change in dimer formation, within experimental error, in the absence of Ca^{2+}. For instance, at 3.8 and 9.5 μM, PDP1c peak centers were observed at 3.67 and 4.14 S in the absence of Ca^{2+} and at 3.72 and 4.28 S (Figure 4) when Ca^{2+} was included, respectively. Furthermore, sedimentation profiles were equivalent within experimental error at 9.5 μM PDP1c when 4 mM Mg^{2+} was included in the presence or absence of Ca^{2+}.

The top panels in Figure 5 show the original scans and SEDFIT fit (*38*) using the monomer−dimer model (solid lines) for the sedimentation velocity studies at 3.8, 9.5, and 19.0 μM in the absence of Ca^{2+} (1 mM EGTA). We have fit the data in Figure 4 and the full set of studies in the absence of Ca^{2+} (selected profiles top panels, Figure 5) to a monomer−dimer or monomer−trimer equilibrium. The formation of a monomer−dimer equilibrium is strongly supported. The fits imposed the calculated molecular mass of 52 625 Da for the PDP1c monomer and the estimated values of 3.4 and 5.17 S for the monomer and all dimer, respectively (see Experimental Procedures). In the absence of Ca^{2+}, the average values for the apparent K_d from the four highest concentrations were 8.55 ± 1.3 μM from the SEDFIT fitting (see the data set, Figure 5 legend) and 6.7 ± 2 μM from the SEDPHAT fitting. The global fit derived using SEDPHAT gave a K_d of 6.3 μM (error range of 5.6−7.1 μM). In Figure 4 (with Ca^{2+}), the dashed lines shown at 3.8 and 9.5 μM were obtained when the $g(s^*)$ transformation was performed on the fit obtained using SEDFIT and the monomer−dimer model. When Ca^{2+} was included (Figure 4), SEDPHAT gave a global fit K_d of 9.2 μM (error range of 8.3−10.5 μM). Simulations with SedAnal also supported a similar self-association affinity.

We also assessed the sedimentation equilibrium profiles at three concentrations of PDP1c at four speeds (see Experimental Procedures). The bottom panels in Figure 5 show selected results and lines from a global fit of those data; the global fit gave a K_d of 5.50 μM (error range of 4.7−6.4 μM) for the monomer−dimer equilibrium. This K_d estimate is somewhat lower than that found by the various sedimentation velocity analyses; this is probably due to the experiment being conducted at a lower temperature, 4 °C rather than 20 °C. A global fit of the data with a monomer−trimer model gave a much poorer fit (larger residuals). When the data are globally fit with these models, not using a weighted fit, the rms error that is obtained is >3-fold larger for the dimer−trimer model ($0.008\Delta A_{280}$ vs $0.027\Delta A_{280}$ for trimer model). When the data were fit with a weighted fit by the two models (data shown for the monomer−dimer fit in the bottom panels of Figure 5), the weighted variance was 2.34-fold larger for the monomer−trimer model (reduced χ^2 values of 32.5 vs 13.9 for the dimer model). With the monomer−trimer model, the K_d obtained was 1.85×10^{-10} M^2 (error range of $1.55-2.2 \times 10^{-10}$ M^2).

On the basis of the combination of the sedimentation velocity and equilibrium analyses, we conclude that PDP1c subunits reversibly associate as a dimer with a K_d of 8.0 ± 2.5 μM at 20 °C. Association of PDP1c with the PDP1r subunit must prevent or greatly hinder this interaction since PDP1 is a stable heterodimer. We would note that the affinity of PDP1c in self-association is weaker than the affinity for the L2 domain based on the affinity retardation studies described above. That conclusion is also supported by results, below.

Analysis of the Oligomeric State of PDP1c·L2 Complex by Sedimentation Velocity. The finding that PDP1c forms a monomer−dimer equilibrium raised the question of whether PDP1c as a monomer, a dimer, or both states interacts with the L2 domain in the presence of Ca^{2+}. This was analyzed by sedimentation velocity studies. Panels A and B of Figure 6 show $g(s^*)$ profiles derived from sedimentation velocity studies conducted using 38 (A) and 3.8 μM (B) PDP1c monomer; 4 mM Mg^{2+} was included in all these studies. Panel A shows sedimentation profiles for PDP1c (alone), 82 μM L2 (alone), and the combination of these components in both the absence (0.5 mM EGTA) and presence of Ca^{2+} (0.2 mM). At the 10-fold lower levels, panel B shows these profiles but for clarity does not include the studies for the combination in the absence of Ca^{2+}. In the absence of free Ca^{2+}, the profiles for L2 and PDP1c appear to equal the summation of the $g(s^*)$ profiles for each sedimented alone. This again indicates that there was not a significant interaction between L2 [S_{20w} = 1.5 S (*34*)] and PDP1c in the absence of Ca^{2+}. Inclusion of Ca^{2+} with L2 and PDP1c resulted in a peak with a sedimentation rate [peak at 4.3 S in the $g(s^*)$ profile] lower than that of PDP1c alone (peak at 4.9 S). At the same time, there was an increase over PDP1c in the height of this peak and a decrease in the trailing free L2 due to complex formation. These data support L2 preferentially binding to the PDP1c monomer. At 10-fold

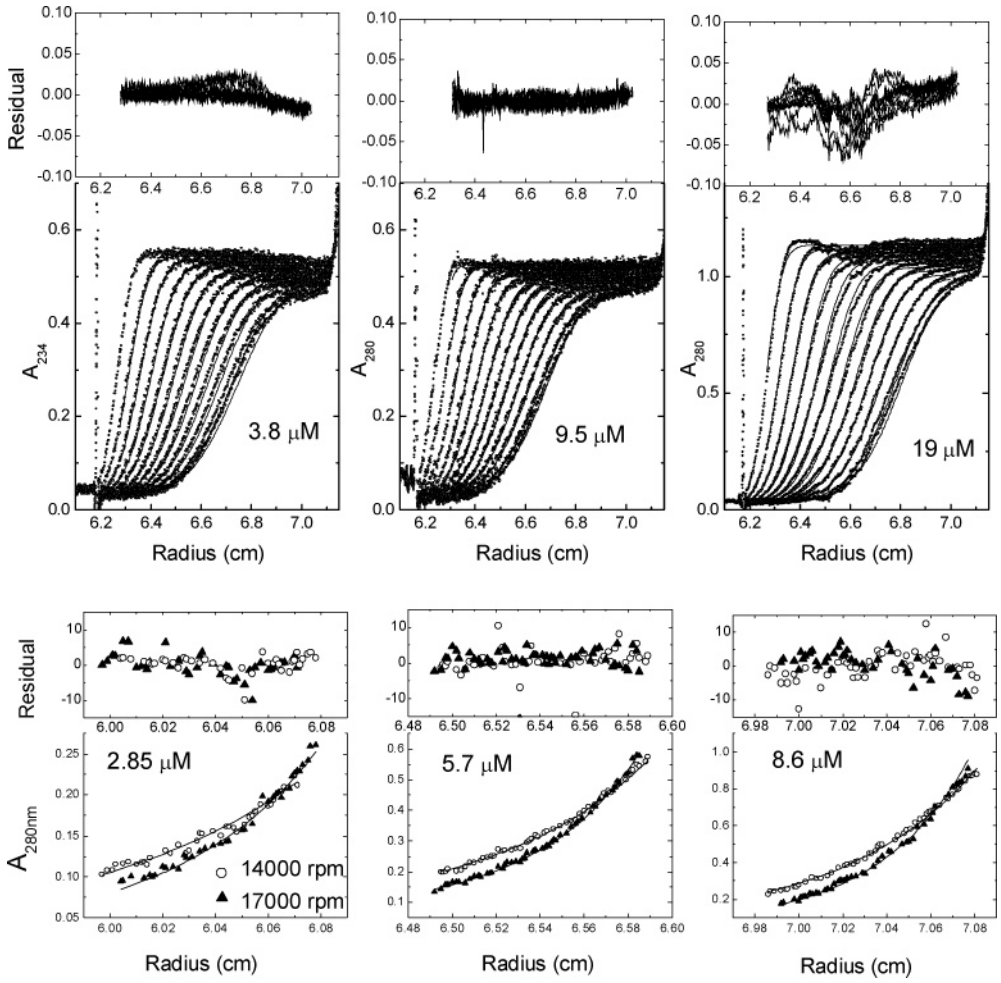

FIGURE 5: Sedimentation velocity profiles for PDP1c in the absence of free Ca^{2+} (top panels) and sedimentation equilibrium profiles for PDP1c (bottom panels). Sedimentation velocity studies were performed at 40 000 rpm and 20 °C in a buffer containing 0.5 mM EGTA at the same concentrations given in Figure 4. In the top panels, the sedimentation velocity scans are shown for the indicated concentrations along with the global fit shown for each run (—) that was obtained by the SEDPHAT program with the monomer−dimer model (K_d = 6.3 μM). SEDFIT modeling of the profiles with the monomer−dimer equilibrium for the results obtained with 3.8, 9.5, 19, and 38 μM PDP1c yielded K_d values (error ranges) of 9.75 (8.65−10.9 μM), 9.5 (8.5−10.45 μM), 7.75 (6.75−8.7 μM), and 7.2 μM (5.8−8.6 μM), respectively. The bottom panels show selected sedimentation equilibrium profiles. Sedimentation equilibrium was sequentially established at 8000, 10 000, 14 000, and 17 000 rpm at 4 °C. The global fit (—) is shown for sedimentation of the indicated PDP1c concentrations at the two higher speeds. Other conditions were as described in Experimental Procedures.

lower levels of components (e.g., 3.8 μM PDP1c and 8.2 μM L2), there was a transition to the PDP1c·Ca^{2+}·L2 complex sedimenting faster than PDP1c alone (panels B of Figure 6). This transition from faster to slower sedimentation of PDP1c is due to the decrease in the PDP1c dimer at this lower level. These findings suggest that L2 preferentially or exclusively binds the PDP1c monomer and does so with an affinity that is tighter than the self-association by PDP1c monomers.

To further evaluate whether a tight 1:1 complex is formed by L2 and the PDP1c monomer, sedimentation velocity profiles were characterized for 7.6 μM PDP1c with 8.4 (1:1.05 ratio) or 16.8 μM L2 (1:2.1 ratio) (Figure 6C) and at a 3-fold lower level at the 1:1.05 ratio (Figure 6D). Increasing the ratio of L2 caused only a slight increase in the rate of sedimentation of the PDP1c·Ca^{2+}·L2 complex, and the level of free L2 increased at the higher level (Figure 6C). Similarly, the 3-fold reduction in the level of PDP1c and L2 caused only a small decrease in the rate of sedimentation of the complex, and multiplying the observed area by 3 gave an integrated area nearly as large as that observed at the higher concentration. These data support a 1:1 complex of the PDP1c monomer and L2 and a submicromolar binding affinity. A K_d between 0.6 and 0.9 μM is roughly estimated based on the changes in total concentrations derived from the $g(s^*)$ distributions in panels C and D (e.g., $3 \times 0.162A_{280}$ for the lower and $0.502A_{280}$ for the higher concentration at the 1:1.05 ratio and 0.515 for the 2.1:1 ratio in the range of 3.0−7.5 S; $0.433A_{280}$ for the near equivalent range, 2.5−7.5 S for PDP1c, alone). The changes in S_{wa} support tighter binding of L2 to PDP1c (K_d < 0.2 μM). A similar affinity for binding of PDP1c to the L2 domains of E2 is derived below.

With the simplifying assumption of treating the PDP1c·Ca^{2+}·L2 complex as a single species in the 3.2−5.45 S range, a molecular mass of 63.9 kDa is estimated from the $S_{20,w}$ of 4.24 S for the $g(s^*)$ distribution observed with 7.6 μM PDP1c and 8.4 μM L2. This calculation derives information about diffusion from the width of the Gaussian. That width can be influenced by association−dissociation processes; however, the impact should not be very large for a complex that is this tight. The estimated MW is close to the calculated MW

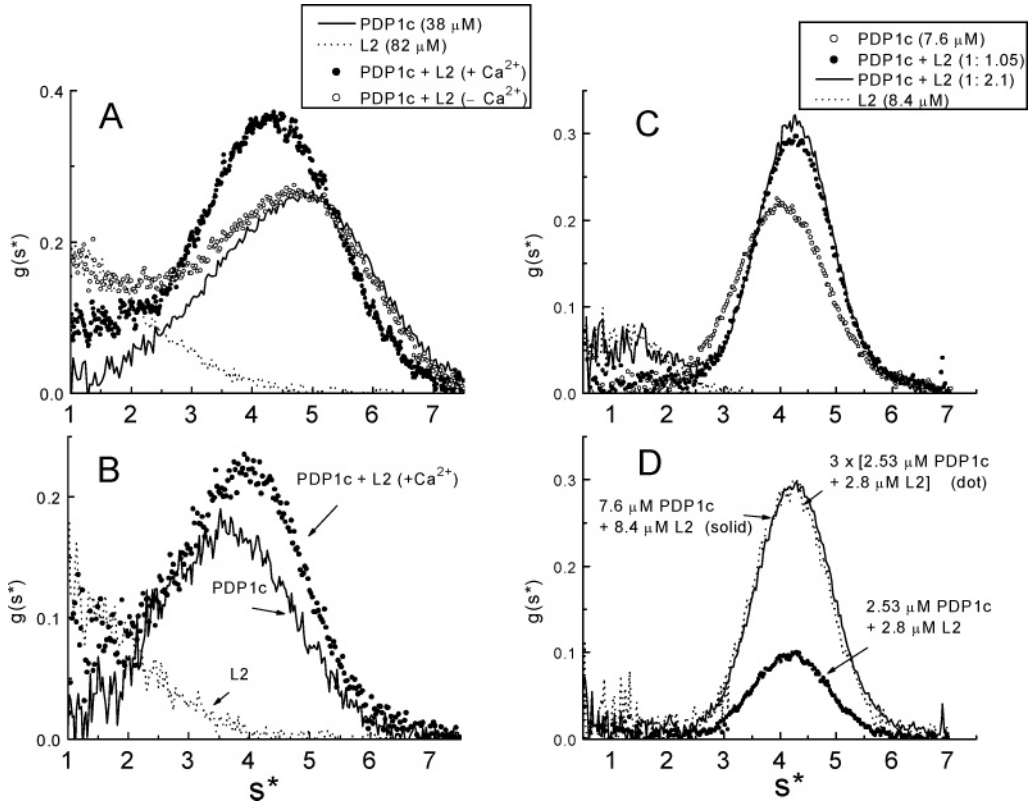

FIGURE 6: $g(s^*)$ profiles for sedimentation velocity studies with L2 and PDP1c. In panels A and B, sedimentation velocity studies were conducted at 40 000 rpm at 20 °C using a buffer containing 10 mM Mg^{2+}. Panel A shows $g(s^*)$ profiles from sedimentation velocity studies conducted with 38 μM PDP1c monomer and 82 μM L2, alone, and for the combination in both the absence (1.0 mM EGTA) and presence of Ca^{2+} (0.1 mM). Panel B shows the $g(s^*)$ profiles for studies with 3.8 μM PDP1c and 8.2 μM L2 in the presence of Ca^{2+}; the sedimentation patterns obtained for the combination in the absence of free Ca^{2+} are not included for visual clarity because there was considerable overlap with the data for PDP1c alone. The sedimentation velocity studies shown in panels C and D were conducted at 55 000 rpm and 20 °C. Panel C shows $g(s^*)$ profiles for 7.6 μM PDP1c alone and combined with 8.4 or 16.8 μM L2 as well as the profile for 8.4 μM L2, alone. Panel D shows the $g(s^*)$ profile for the 1.05:1 L2:PDP1c ratio using 3-fold lower levels of PDP1c and compares three times× this profile to the one obtained with the 3-fold higher level.

of 65.604 kDa for the PDP1c·L2 complex, based on the amino acid sequence of these proteins. This further supports the formation of a 1:1 complex by the monomeric form of PDP1c and L2. The transition to a monomer suggests either that the tight binding by L2 occurs with a region of the surface of PDP1c that participates in forming the PDP1c dimer or that the Ca^{2+}-aided interaction induces a conformational change in PDP1c that markedly weakens self-association.

Binding of PDP1c to the E2 60mer. The capacity of the E2 60mer to bind PDP1c was evaluated when the level of the PDP1c monomer was varied from 17.5 to 175 PDP1c molecules per E2 60mer (0.1085 μM) (Figure 7A). The extent of binding in each experiment was assessed using the change in peak area of $g(s^*)$ versus s^* of the leading peaks, the change in the level trailing (free PDP1c), and the increase in absorbance of the leading peak due to PDP1c binding. Figure 7B plots the results of all the analyses of the concentrations estimated from the $g(s^*)$ peaks. This analysis gave results that were within the experimental error of the other two analyses. When the data were fit by one class of binding sites and fit with a simple least-squares analysis (dashed line in Figure 7B), a K_d of ~0.22 μM for PDP1c binding at ~41 sites was estimated. A weighted least-squares analysis giving higher binding levels more influence (solid line in Figure 7B) yielded a K_d of 0.28 ± 0.9 μM for binding at a maximum of 46.6 ± 4.5 PDP1c molecules bound per E2 60mer. A closer fit of the data is obtained using two classes of sites; however, several combinations of sites per K_d give results falling within experimental error when two classes of sites are assumed to always be present. With an assumption that weaker sites develop sequentially due to crowding at the E2 surface, a good fit is obtained for 39 sites with a K_d of 0.19 μM and 11 sites with a K_d of 0.52 μM. Regardless, the results establish that a large complement of PDP1c (>40) can be simultaneously bound by the E2 60mer, and most bind with a K_d of <0.35 μM. These results are in good agreement with the K_d range estimated for PDP1c binding to the free L2 domain. With standard conditions used in the ^{32}P-labeled phosphate release assay (<0.4 PDP1c monomer/E2 60mer with E2 at 0.11 μM), ~90% of PDP1c is predicted to be bound by E2 based on the fit to one class of sites. This is consistent with the modest but definite increase in rates observed with PDP1c when higher levels of the E2·P−E1 complex are used as the substrate (*17*).

Binding of Ca^{2+} to PDP1c, L2, or Both Analyzed by Isothermal Titration Calorimetry (ITC). To evaluate whether PDP1c, L2, or only the combination is a Ca^{2+}-binding protein, Ca^{2+} binding was assessed using ITC. In the absence of Mg^{2+}, titration of PDP1c (38.5 μM) with Ca^{2+} gave a small exothermic heat change (data not shown). The incremental contribution to the integrated signal decreased gradually even after addition of 2.0 Ca^{2+} ions per PDP1c. In the presence of 1 mM Mg^{2+}, binding of Ca^{2+} to PDP1c was not

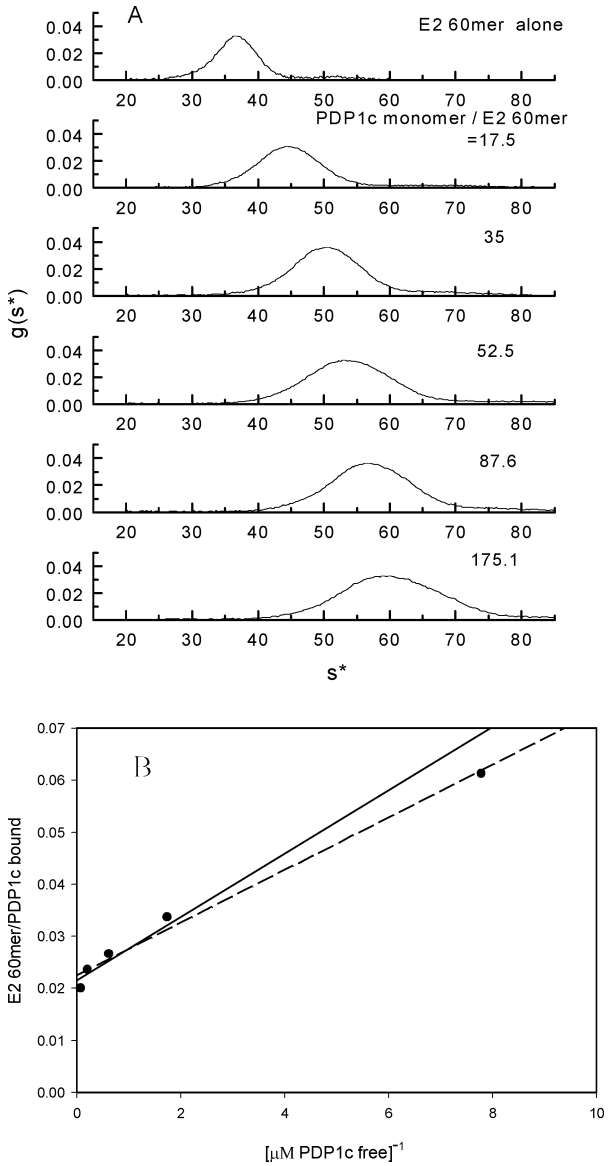

FIGURE 7: Changes in sedimentation of E2 due to binding of increasing PDP1c concentration (A) and analysis of PDP1c binding (B). The $g(s^*)$ profiles derived from sedimentation velocity studies conducted with the E2 60mer (0.1085 μM), alone, and this level of E2 with increasing with PDP1c added at the indicated monomer: E2 60mer ratio. Data were analyzed and fit as described in Experimental Procedures. Panel B is a Klotz plot of the estimates of bound and free PDP1c made from the increase in protein concentration in the $g(s^*)$ peak beyond that due to E2. The dashed line is a simple least-squares analysis; the solid line is a weighted analysis that reduces the impact of the estimate of bound PDP1c at the lowest PDP1c level.

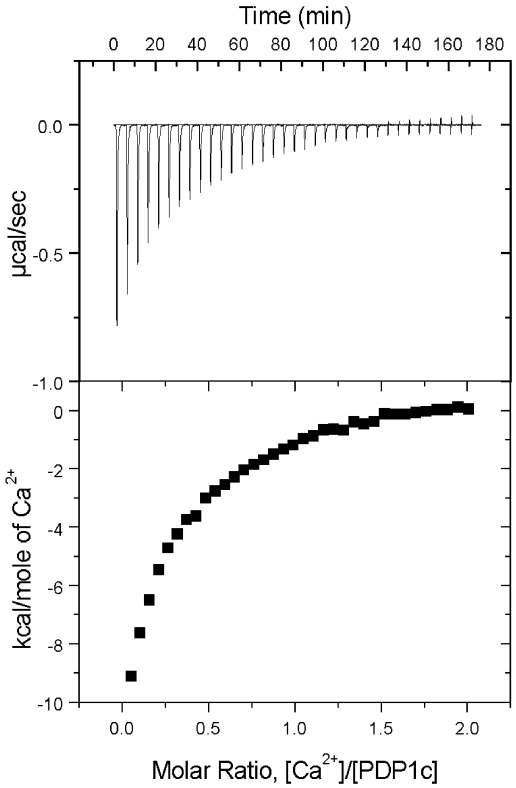

FIGURE 8: Isothermal calorimetric titration of PDP1c and L2 with Ca^{2+}. ITC was performed with a solution equilibrated at 30 °C containing 38.5 μM PDP1c,100 μM L2, and 1 mM Mg^{2+} using 35 automatic injections of 6.68 μL of 0.397 mM Ca^{2+}. The top panel shows the isothermal heat changes, and the bottom panel shows the integrated heat released, both as a function of the increasing Ca^{2+}:PDP1c ratio. Other conditions were as described in Experimental Procedures.

detected by ITC (data not shown). These results suggest that, in the absence of Mg^{2+}, Ca^{2+} binds weakly at the Mg^{2+} binding site on PDP1c. There was no heat change when Ca^{2+} was added to the L2 domain (100 μM) in absence or presence of Mg^{2+} (data not shown). Modest variation in pH and ionic strength did not change the above patterns, so it is unlikely that the lack of detection of a Ca^{2+} interaction with L2 or PDP1c was due to canceling of endothermic and exothermic changes. However, that possibility cannot be completely excluded.

On the other hand, with Mg^{2+} present, titration of Ca^{2+} into a solution containing both PDP1c (38.5 μM) and L2 (100 μM) yielded exothermic heat changes as shown in the top panel of Figure 8. The bottom panel of Figure 8 plots the integrated heat as a function of the ratio of Ca^{2+} to PDP1c. The magnitude of the peaks, which correspond to the heat released after each injection of Ca^{2+}, decreased in a near-hyperbolic fashion and reached saturation at a molar Ca^{2+}:PDP1c ratio of 1. These data indicate that a tight Ca^{2+} binding site was formed in the presence of both PDP1c and the L2 domain. The decreasing signal probably reflects more than one process contributing to the net equilibrium heat that is being generated upon each injection of Ca^{2+}, with an endothermic change increasingly reducing the net heat change. Besides the gain in interactions as the PDP1c·Ca^{2+}·L2 complex forms, thermal changes are likely to result from re-equilibration of the PDP1c monomer−dimer equilibria (above). The various contributions to the ITC titration curve are too complex to allow a definite analysis (best-fit models) for the contributing binding isotherms via the Origin software supplied with the instrument.

Similarly, in the absence of Ca^{2+}, titration of L2 into a PDP1c solution gave little, if any, heat change compared to the heat of dilution of L2 into the dialysis buffer with PDP1c omitted (data not shown). This again indicates that in the absence of Ca^{2+}, the L2·PDP1c interaction is either very weak or not happening. Titration of L2 into a PDP1c solution containing excess Ca^{2+} produced an exothermic heat change similar to that in Figure 8, further demonstrating that the Ca^{2+}-dependent interaction between L2 and PDP1c can be detected by ITC (data not shown). Again, the signal decreased with increasing increments of L2, suggesting that

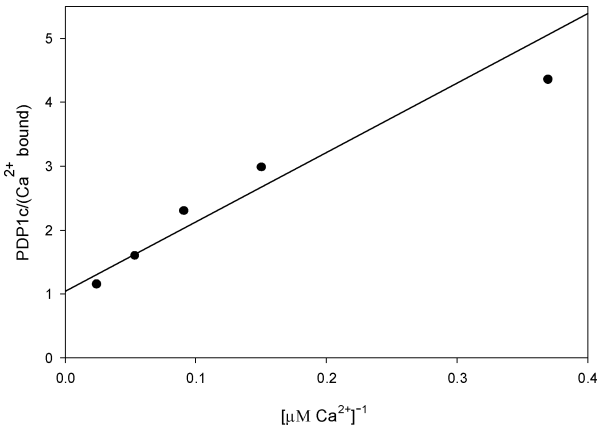

FIGURE 9: Klotz plot of binding of $^{45}Ca^{2+}$ to PDP1c. $^{45}CaCl_2$ was added to final concentrations of 5−50 μM to solutions containing 10 μM PDP1c and 30 μM wild-type L2 or a control lacking protein. The corrected levels of bound Ca^{2+} were estimated from the filtrate following ultrafiltration which was carried out and analyzed as described in Experimental Procedures.

competing thermodynamic changes were occurring. All of the above ITC results combine to strongly suggest that development of a tight Ca^{2+} binding site requires both PDP1c and L2.

$^{45}Ca^{2+}$ Binding Studies. Although ITC did not detect tight binding of Ca^{2+} to PDP1c or L2, alone, those studies did not completely eliminate the possibility that Ca^{2+} binding causes conformational changes which compensate for the heat of binding of Ca^{2+} so that no net heat change was observed. Therefore, $^{45}Ca^{2+}$ binding was directly evaluated using ultrafiltration. The ultrafiltration membrane, at all concentrations, removed 8.0 ± 0.5% of the free Ca^{2+} passing through the membrane in the no enzyme controls. Our analysis assumes that this also occurred in the presence of protein components when the free Ca^{2+} passed through the membrane. No binding of $^{45}Ca^{2+}$ to either PDP1c or L2, alone, was detected. Ca^{2+} binding occurred with the combination of PDP1c and L2. Figure 9 shows a Klotz plot for binding of $^{45}Ca^{2+}$ to 10 μM PDP1c in the presence of 30 μM L2. Binding appeared to occur at one site with an apparent binding constant of 10 ± 3 μM. The level of $^{45}Ca^{2+}$ in the retentates exhibited the expected increase in Ca^{2+} concentration; however, the small errors in measuring retentate volumes led to somewhat larger deviations than using the filtrates for estimating the extent of binding. The estimated binding affinity for Ca^{2+} is weaker than predicted on the basis of the K_{act} derived for Ca^{2+} from activity studies and the influence of Ca^{2+} on binding to the gel-bound GST−L2 protein, above, when the concentration of free Ca^{2+} was controlled with EGTA-Ca^{2+} buffers. Similar but larger discrepancies were observed with the PDP1 heterodimer (*14*).[6]

Overall Analysis. We have obtained strong evidence that both PDP1c and the L2 domain of E2 act in concert to form a site for tightly binding Ca^{2+}. Neither PDP1c nor L2 has a region of sequence that is predicted to form a standard Ca^{2+} binding domain [EF-hand (*48*) or C_2 (*49*) domains]. Furthermore, neither the three-dimensional structure of L2 (*31*) nor the folded backbone structure of PDP1c[3] contains a structural fold resembling the folds (*48*, *49*) of these most common domains for tightly binding Ca^{2+}. Therefore, our results suggest that a novel tight Ca^{2+} binding site is formed by these proteins. As indicated in the introductory section, site-specific mutations revealed an acidic cluster in L2 that is critical for the formation of the PDP1c·Ca^{2+}·L2 complex.

Since, on the basis of the ITC and $^{45}Ca^{2+}$ binding studies, L2 and PDP1c are needed for tight Ca^{2+} binding, a weak interaction must precede the formation of the tight Ca^{2+} binding site. The initial weak interaction may involve either L2 weakly interacting with PDP1c or weak Ca^{2+} binding. Regardless of the pathway, the stable complex with tightly held Ca^{2+} is likely to involve either binding of Ca^{2+} to an induced site in PDP1c (given L2's structure induction of the tight site in L2 seems unlikely) or binding at a bridge position between PDP1c and L2. The latter might involve one or more group in the acidic cluster detected in L2 (*26*) by mutation mapping which includes three glutamates (residues 162, 179, and 182). Glu182 was found to be essential for this interaction even though it was not important in other roles that we have evaluated (use of L2 as an E1 substrate or activation of PDK3 by L2). Therefore, Glu182 in L2 is a likely candidate for participating in what may be a limited Ca^{2+} bridge between PDP1c and L2. Only a three-dimensional structure of the complex will allow this to be definitively defined.

Regardless of the mechanism, the studies with EGTA-Ca buffers indicate that Ca^{2+} activates PDP1c with an apparent K_{act} of ≈3 μM. A higher equilibrium K_d (10 ± 3 μM) was obtained in $^{45}Ca^{2+}$ binding studies. It is not clear whether nonspecific binding of Ca^{2+} (leading to the actual free $^{45}Ca^{2+}$ being reduced) fully explains this difference between the estimated K_{act} and K_d. There was constant binding by the filter (above); minimal nonspecific binding is otherwise expected since the study was conducted with homogeneous PDP1c and L2 prepared in Chelex-treated Hepes-Tris buffer to which 5 mM $MgCl_2$ and 60 mM KCl were added. The apparent K_{act} for Ca^{2+} was determined under conditions of catalytic turnover. However, the studies of binding of PDP1c to the gel-retained GST−L2 protein using EGTA-Ca buffers indicated that Ca^{2+} levels near 1 μM are very effective in supporting binding of the catalytic subunit to the GST−L2 protein in the absence of turnover (E2 and P-E1) or Mg^{2+}. We have prepared only 1 mg amounts of purified PDP1 and, therefore, could not perform ITC studies and did not re-evaluate Ca^{2+} binding by this heterodimer. Teague et al. (*14*) suggested that PDP1 has a Ca^{2+} binding site and that a second site is created when PDP1 interacts with E2. Their studies yielded binding affinities that were much weaker[6] than the apparent K_{act} observed herein and, for saturating Mg^{2+} concentrations, in earlier studies (*10*, *29*). In the studies with the gel-bound GST−L2 protein and EGTA-Ca buffers, inclusion of elevated Mg^{2+} concentrations led to near-

[6] Using flow dialysis to estimate the level of binding of $^{45}Ca^{2+}$ in the presence of 1.5 mM Mg^{2+}, a binding site on PDP1 alone with an apparent K_d of 55 μM Ca^{2+} and a second binding site with E2 and PDP1 with an apparent K_d of 41 μM were detected (*14*). Back-titration with EGTA, to a lower $^{45}Ca^{2+}$ concentration, yielded much lower estimates of 7.5 and 5 μM for these two sites, respectively. The basis for the large variation in values was not understood. We did not detect Ca^{2+} binding with PDP1c using a higher Mg^{2+} concentration (4 mM). It is uncertain whether Ca^{2+} binding might be occurring at the active site which is probably a bi-Mg^{2+} binding site like that found in the related protein phosphatase 2C (*47*) or whether the presence of the PDP1r subunit led to an additional Ca^{2+} binding site. Since PDP1c, alone, binds in a Ca^{2+}-dependent manner to E2 and the L2 domain, any site on PDP1r is not required for complex formation.

micromolar Ca^{2+} concentrations, also supporting tight binding to L2 of the PDP1 heterodimer.

We have found that isolated PDP1c establishes a reversible monomer−dimer equilibrium ($K_d \approx 8\ \mu M$) and that formation of the tighter PDP1c·Ca^{2+}·L2 complex captures PDP1c as a monomer. The affinity for PDP1c binding to free L2 seems to be similar to the affinity for L2 sites in the E2 60mer ($K_d \simeq 0.3\ \mu M$ at saturating Ca^{2+} concentrations). Clearly, binding of PDP1r to PDP1c also prevents the association between PDP1c subunits since PDP1 is a stable heterodimer (*13*, *14*). Since association with PDP1r or E2 hinders dimer formation by PDP1c, it would seem that a PDP1c dimer could form inside the mitochondrial matrix only when Ca^{2+} levels are low (preventing binding to E2) and when either less PDP1r than PDP1c is present or PDP1r is sequestered away from PDP1c. PDP1 does not tend to aggregate at <0.5 mg/mL, but it is otherwise a very sticky protein that binds to surfaces, including dialysis tubing (cellulose). It seems clear that the 96 kDa PDP1r subunit makes a major contribution to this tendency of PDP1 to bind to surfaces; PDP1r possibly has a role in binding to some site separate from PDC. Pluronic F68 is used in all studies with PDP1 and greatly reduces the extent of nonspecific binding.

Our results further support the concept that the PDP1r subunit alters the properties of and contributes to cross talk between the metal binding sites in the PDP1c subunit. Comparing the K_m values of PDP1 and PDP1c for Mg^{2+} indicated that PDP1r increases the K_m of PDP1 for Mg^{2+} (*7*, *17*). Ca^{2+} reduces the K_m of PDP1 for Mg^{2+} (*17*, *28*). We have found at saturating Mg^{2+} concentrations that there is a 3-fold reduction in the apparent K_{act} for Ca^{2+} of PDP1 (but not PDP1c) even while Mg^{2+} causes a broadening in the Ca^{2+} concentration range over which the level of activation increases. This again indicates that PDP1r has a role in fostering a Mg^{2+}-dependent increase in the sensitivity to Ca^{2+}. PDP1r presumably causes or stabilizes a conformational change in PDP1c that elicits the increased sensitivity of PDP1c for Ca^{2+} as the Mg^{2+} concentration is elevated. This effect may require the active site of PDP1c [assumed to be a bi-Mg^{2+} site based on the only protein phosphatase 2C class three-dimensional structure (*47*)] to be fully occupied by Mg^{2+} ions. Altogether, the observations described above indicate that PDP1r plays a mediator role between the Mg^{2+} and Ca^{2+} binding sites with the responsiveness to one metal being enhanced by an increase in the level of the other metal. Spermine-induced reduction in the K_m of PDP1 for Mg^{2+} acts to reverse the effect of PDP1r in elevating this K_m. At the same time, spermine contributes to a decrease in the apparent K_{act} of PDP1 for Ca^{2+} at subsaturating but not at saturating Mg^{2+} concentrations (*28*) since K_{act} is already low (ref *10* and data herein). Therefore, although binding of PDP1c to L2 creates the tight Ca^{2+} binding site, the PDP1r subunit fosters a connection of this site to the Mg^{2+} site on PDP1c and makes both sites sensitive to spermine.

ACKNOWLEDGMENT

We thank Shane Kasten, Xiaohua Yan, Haiying Bao, and John Kurche for their contributions to the preparation of E1, PDK2, E2, E2·E3BP, and E3 used in these studies.

REFERENCES

1. Reed, L. J. (1974) Multienzyme complexes, *Acc. Chem. Res. 7*, 40−46.
2. Roche, T. E., and Cox, D. J. (1996) Multifunctional 2-oxo acid dehydrogenase complexes, in *Channeling in Intermediary Metabolism* (Agius, L., and Sherratt, H. S. A., Eds.) pp 115−132, Portland Press Ltd., London.
3. Roche, T. E., Baker, J., Yan, X., Hiromasa, Y., Gong, X., Peng, T., Dong, J., Turkan, A., and Kasten, S. A. (2001) Distinct regulatory properties of pyruvate dehydrogenase kinase and phosphatase isoforms, *Prog. Nucleic Acid Res. Mol. Biol. 70*, 33−75.
4. Gudi, R., Bowker-Kinley, M. M., Kedishvili, N. Y., Zhao, Y., and Popov, K. M. (1995) Diversity of the pyruvate dehydrogenase kinase gene family in humans, *J. Biol. Chem. 270*, 28989−28994.
5. Rowles, J., Scherer, S. W., Xi, T., Majer, M., Nickle, D. C., Rommens, J. M., Popov, K. M., Harris, R. A., Riebow, N. L., Xia, J., Tsui, L.-C., Bogardus, C., and Prochazka, M. (1996) Cloning and characterization of PDK4 on 7q21.3 encoding a fourth pyruvate dehydrogenase kinase isozyme in human, *J. Biol. Chem. 271*, 22376−22382.
6. Steussy, C. N., Popov, K. M., Bowker-Kinley, M. M., Sloan, R. B., Harris, R. A., and Hamilton, J. A. (2001) Structure of pyruvate dehydrogenase kinase. Novel folding pattern for a serine protein kinase, *J. Biol. Chem. 276* 37443−37450.
7. Lawson, J. E., Niu, X.-D., Browning, K. S., Trong, H. L., Yan, J., and Reed, L. J. (1993) Molecular cloning and expression of the catalytic subunit of bovine pyruvate dehydrogenase phosphatase and sequence similarity with protein phosphatase 2C, *Biochemistry 32*, 8987−8993.
8. Huang, B., Gudi, R., Wu, P., Harris, R. A., Hamilton, J., and Popov, K. M. (1998) Isozymes of pyruvate dehydrogenase phosphatase. DNA-derived amino acid sequences, expression, and regulation, *J. Biol. Chem. 273*, 17680−17688.
9. Reed, L. J., and Damuni, Z. (1987) Mitochondrial protein phosphatases, *Adv. Protein Phosphatases 4*, 59−76.
10. Denton, R. M., Randle, P. J., and Martin, B. R. (1972) Stimulation by calcium ions of pyruvate dehydrogenase phosphate phosphatase, *Biochem. J. 128*, 161−163.
11. Reed, L. J., Lawson, J. E., Niu, X.-D., and Yan, J. (1996) Pyruvate dehydrogenase phosphatase, in α *Keto Acid Dehydrogenase Complexes* (Patel, M. S., Roche, T. E., and Harris, R. A., Eds.) pp 131−138, Birkhäuser Verlag Press, Basel, Switzerland.
12. Pettit, F. H., Roche, T. E., and Reed, L. J. (1972) Function of calcium ions in pyruvate dehydrogenase phosphatase activity, *Biochem. Biophys. Res. Commun. 49*, 563−571.
13. Pratt, M. L., Maher, J. F., and Roche, T. E. (1982) Purification of bovine kidney and heart pyruvate dehydrogenase phosphatase on Sepharose derivatized with the pyruvate dehydrogenase complex, *Eur. J. Biochem. 125*, 349−355.
14. Teague, W. M., Pettit, F. H., Wu, T.-L., Silberman, S. R., and Reed, L. J. (1982) Purification and properties of pyruvate dehydrogenase phosphatase from bovine heart and kidney, *Biochemistry 21*, 5585−5592.
15. Chen, G., Wang, L., Liu, S., Chang, C., and Roche, T. E. (1996) Activated function of the pyruvate dehydrogenase phosphatase through Ca^{2+}-facilitated binding to the inner lipoyl domain of the dihydrolipoyl acetyltransferase, *J. Biol. Chem. 271*, 28064−28070.
16. Lawson, J. E., Park, S. H., Mattison, A. R., Yan, J., and Reed, L. J. (1997) Cloning, expression and properties of the regulatory subunit of bovine pyruvate dehydrogenase phosphatase, *J. Biol. Chem. 272*, 31625−31629.
17. Yan, J., Lawson, J. E., and Reed, L. J. (1996) Role of the regulatory subunit of bovine pyruvate dehydrogenase phosphatase, *Proc. Natl. Acad. Sci. U.S.A., 93*, 4953−4956.
18. Damuni, Z., Humphreys, J. S., and Reed, L. J. (1987) Stimulation of pyruvate dehydrogenase phosphatase activity by polyamines, *Biochem. Biophys. Res. Commun. 124*, 95−99.
19. Thekkumkara, T. J., Ho, L., Wexler, I. D., Pons, G., Lui, T.-C., and Patel, M. S. (1988) Nucleotide sequence of a cDNA for the dihydrolipoamide acetyltransferase component of human pyruvate dehydrogenase complex, *FEBS Lett. 240*, 45−48.
20. Yang, D., Song, J., Wagenknecht, T., and Roche, T. E. (1997) Assembly and full functionality of recombinantly expressed dihydrolipoyl acetyltransferase component of the human pyruvate dehydrogenase complex, *J. Biol. Chem. 272*, 6361−6369.
21. Hiromasa, Y., Fujisawa, T., Aso, Y., and Roche, T. E. (2004) Organization of the cores of the mammalian pyruvate dehydro-

genase complex formed by E2 and E2 plus the E3-binding protein and their capacities to bind the E1 and E3 components, *J. Biol. Chem. 279*, 6921−6933.
22. Jilka, J. M., Rahmatullah, M., Kazemi, M., and Roche, T. E. (1986) Properties of a newly characterized protein of the bovine kidney pyruvate dehydrogenase complex, *J. Biol. Chem. 261*, 1858−1867.
23. Rahmatullah, M., Gopalakrishnan, S., Andrews, P. C., Chang, C. L., Radke, G. A., and Roche, T. E. (1989) Subunit associations in the mammalian pyruvate dehydrogenase complex: Structure and role of protein X and the pyruvate dehydrogenase component binding domain of the dihydrolipoyl transacetylase component, *J. Biol. Chem. 264*, 2221−2227.
24. Harris, R. A., Bowker-Kinley, M. M., Wu, P., Jeng, J., and Popov, K. M. (1997) Dihydrolipoamide dehydrogenase-binding protein of the human pyruvate dehydrogenase complex. DNA-derived amino acid sequence, expression, and reconstitution of the pyruvate dehydrogenase complex, *J. Biol. Chem. 272*, 19746−19751.
25. Yang, D., Gong, X., Yakhnin, A., and Roche, T. E. (1998) Requirements for the adaptor protein role of dihydrolipoyl acetyltransferase in the upregulated function of the pyruvate dehydrogenase kinase and pyruvate dehydrogenase phosphatase, *J. Biol. Chem. 273*, 14130−14137.
26. Turkan, A., Gong, X., Peng, T., and Roche, T. E. (2002) Structural requirements within the lipoyl domain for the Ca^{2+}-dependent binding and activation of pyruvate dehydrogenase phosphatase isoform 1 or its catalytic subunit, *J. Biol. Chem. 277*, 14976−14985.
27. Choi, W. S., Yan, J., McCarthy, D. B., Seung, H. P., and Reed, L. J. (2000) One-step purification of the recombinant catalytic subunit of pyruvate dehydrogenase phosphatase, *Protein Expression Purif. 20*, 128−131.
28. Thomas, A. P., Diggle, T. A., and Denton, R. M. (1986) Sensitivity of pyruvate dehydrogenase phosphatase to Mg^{2+} ions, *Biochem. J. 238*, 83−91.
29. Roche, T. E., and Cate, R. L. (1977) Purification of porcine liver pyruvate dehydrogenase complex and characterization of its catalytic and regulatory properties, *Arch. Biochem. Biophys. 183*, 664−677.
30. Karpova, T., Danchuk, S., Kolobova, E., and Popov, K. M. (2003) Characterization of the isozymes of pyruvate dehydrogenase phosphatase: implications for regulation of pyruvate dehydrogenase activity, *Biochim. Biophys. Acta 1652*, 126−135.
31. Howard, M. J., Fuller, C., Broadhurst, R. W., Perham, R. N., Tang, J.-G., Quinn, J., Diamond, A. G., and Yeaman, S. J. (1998) Three-dimensional structure of the major autoantigen in primary biliary cirrhosis, *Gastroenterology 115*, 139−146.
32. Liu, S., Baker, J. C., Andrews, P. C., and Roche, T. E. (1995) Recombinant expression and evaluation of the lipoyl domains of the dihydrolipoyl acetyltransferase component of human pyruvate dehydrogenase complex, *Arch. Biochem. Biophys. 316*, 926−940.
33. Lawlis, V. B., and Roche, T. E. (1980) Effect of micromolar Ca^{2+} on NADH inhibition of bovine kidney α-ketoglutarate dehydrogenase complex and possible role of Ca^{2+} in signal amplification, *Mol. Cell. Biochem. 32*, 147−152.
34. Portzehl, H., Caldwell, P. C., and Ruegg, J. C. (1964) The dependence of contraction and relaxation of muscle fibres from crab MAIA squnado on the internal concentration of free calcium ions, *Biochim. Biophys. Acta 79*, 581−591.
35. Hiromasa, Y., and Roche, T. E. (2003) Facilitated interaction between the pyruvate dehydrogenase kinase isoform 2 and the dihydrolipoyl acetyltransferase, *J. Biol. Chem. 278*, 33681−33693.
36. Gong, X., Peng, T., Yakhnin, A., Zolkiewski, M., Quinn, J., Yeaman, S. J., and Roche, T. E. (2000) Specificity Determinants for the Pyruvate Dehydrogenase Component Reaction Mapped with Mutated and Prosthetic Group Modified Lipoyl Domains, *J. Biol. Chem. 275*, 13645−13653.
37. Philo, J. S. (2000) A method for directly fitting the time derivative of sedimentation velocity data and an alternative algorithm for calculating sedimentation coefficient distribution functions, *Anal. Biochem. 279*, 151−163.
38. Stafford, W. F. (1992) Boundary analysis in sedimentation transport experiments: a procedure for obtaining sedimentation coefficient distributions using the time derivative of the concentration profile, *Anal. Biochem. 203*, 295−301.
39. Stafford, W. F. (1994) Sedimentation boundary analysis of interacting systems: use of the apparent sedimentation coefficient distribution function, in *Modern Analytical Ultracentrifugation: Acquisition and Interpretation of Data for Biological and Synthetic Polymer Systems* (Schuster, T. M., and Laue, T. M., Eds.) pp 119−137, Birkhauser, Boston.
40. Stafford, W. F. (2000) Analysis of reversibly interacting macromolecular systems by time derivative sedimentation velocity, *Methods Enzymol. 323*, 303−325.
41. Correia, J. J., Chacko, B. M., Lam, S. S., and Lin, K. (2001) Sedimentation studies reveal a direct role of phosphorylation in Smad3:Smad4 homo- and hetero-trimerization, *Biochemistry 40*, 1473−1482.
42. Schuck, P. (1998) Sedimentation analysis of noninteracting and self-associating solutes, using numerical solutions to the Lamm equation, *Biophys. J. 75*, 1503−1512.
43. Schuck, P. (2003) On the analysis of protein self-association by sedimentation velocity analytical ultracentrifugation, *Anal. Biochem. 320*, 104−124.
44. Wiseman, T., Williston, S., Brands, J. F., and Lin, L.-N. (1989) Rapid measurement of binding constants and heats of binding using a new titration calorimeter, *Anal. Biochem. 179*, 131−137.
45. Indyk, L., and Fisher, H. F. (1998) Theoretical aspects of isothermal titration calorimetry, *Methods Enzymol. 295*, 350−364.
46. Schittny, J. C. (1994) Affinity retardation chromatography: characterization of the method and its application, *Anal. Biochem. 222*, 140−148.
47. Das, A. K., Helps, N. R., Cohen, P. T. W., and Barford, D. (1966) Crystal structure of the protein serine/threonine phosphatase 2C at 2.0 Å resolution, *EMBO J. 15*, 6798−6809.
48. Kawasaki, H., and Kretsinger, R. (1994) Calcium-binding proteins 1: EF-hands, *Protein Profile 1*, 343−349.
49. Rizo, J., and Sudhof, T. C. (1998) C_2-domains, structure and function of a universal Ca^{2+}-binding domain, *J. Biol. Chem. 273*, 15879−15882.

BI048901Y